https://dx.doi.org/10.21577/0103-5053.20210160

J. Braz. Chem. Soc., Vol. 33, No. 5, 413-424, 2022

Article

Determination of 3,4,5-Trihydroxybenzoic Acid Exploiting a Visible-Light-Driven Photoelectrochemical Platform: Application in Wine and Tea Samples

Kayni C. M. S. Lima,[a] Ridvan N. Fernandes,[a] Clenilton C. dos Santos,[b] Flavio S. Damos,[a] and Rita de Cássia S. Luz*,[a]*

[a]*Departamento de Química, Universidade Federal do Maranhão, 65080-805 São Luís-MA, Brazil*

[b]*Departamento de Física, Universidade Federal do Maranhão, 65080-805 São Luís-MA, Brazil*

The present work is based on the development and application of a photoelectrochemical method for the amperometric determination of 3,4,5-trihydroxybenzoic acid in different samples. The method is based on the use of a photoelectrochemical platform based on a glass slide coated with fluorine-doped tin oxide, which has been modified with cadmium sulfide and poly(D-glucosamine) and subjected to a light-emitting diode (LED) lamp. The photoelectrochemical platform was sensitive to the increase of the concentration of the antioxidant 3,4,5-trihydroxybenzoic acid in the solution. Under the optimized experimental conditions, the photoelectrochemical method presented a linear response for a 3,4,5-trihydroxybenzoic acid concentration ranging from 0.2 up to 500 μmol L^{-1}. The method was applied to 3,4,5-trihydroxybenzoic acid determination in samples of wines and teas with recoveries between 95.88 and 101.72%. The results obtained suggest that the developed platform is a promising tool for quantifying the 3,4,5-trihydroxybenzoic acid.

Keywords: photoelectrochemistry, 3,4,5-trihydroxybenzoic acid, cadmium sulfide, poly(D-glucosamine)

Introduction

Phenolic compounds are important plant metabolites that determine the quality of fruits, vegetables and they are universally present in a wide range of foods and beverages.[1] Phenolic compounds are characterized by the presence of at least one aromatic ring that possesses one or several hydroxyl substituents.[2] Among the most important phenolic compounds, the 3,4,5-trihydroxybenzoic (THBA) or gallic acid stands out as a reference compound present in green tea, black tea, grape and many other plants.[3] It is an important antioxidant compound, and it is well known in the literature for having antioxidant, antimicrobial, anti-inflammatory, anticancer properties and neuroprotective effects.[4-6] Therefore, taking into account the extreme importance of THBA as well as the importance of relating the routine consumption of foods rich in antioxidants for the treatment or prevention of diseases,[7] the development of novel sensitive, rapid, cost-effective, stable and selective analytical methods for the detection and quantification of this phenolic is of high importance. In this sense, the development of novel methodologies requiring a small amount of sample and low-cost instrumentation has attracted the interest of several research groups.[8-11]

In this sense, several methods have been reported for the determination of THBA, such as chromatography analysis,[12,13] flow injection analysis,[14,15] spectrophotometric determination,[16,17] chemiluminescence,[18] and electrochemical methods.[7,19-22] The electrochemical methods show high versatility, sensitivity, low cost and low volume of reagents, and they can be performed fast.

The photoelectrochemical (PEC) methods retain some exquisite properties of electrochemical and optical methods, proving to be a promising strategy for detecting and quantifying different chemical species.[23-25] The PEC methods exploit the ability of semiconductor materials to absorb radiated energy close to or greater than its bandgap energy, resulting in the formation of electron/hole pairs (e^-/h^+).[23,26] Among the most interesting advantages of using PEC methods are high throughput analysis, user-friendliness, portability, high linear response range, low cost, and easy miniaturization.[25,27] For the PEC detection process, the irradiated light acts as a source of excitation to produce an electrical signal (photocurrent or photovoltage), which can be exploited as a detection signal. Therefore,

*e-mail: flavio.damos@yahoo.com; rita_rcsluz@yahoo.com
Editor handled this article: Rodrigo A. A. Muñoz (Associate)

an efficient separation between the excitation source and the detector contributes to reducing the interference from background signals, thus increasing the system's sensitivity.[28,29] In this context, the choice of photoactive materials is of fundamental importance, such that several materials based on semiconductors have been explored in PEC systems.

Cadmium sulfide (CdS) is an important material in the class of II-IV semiconductors. This semiconductor shows a direct optical gap of around 2.42 eV and large bonding energy of excitons,[30,31] presenting itself as a potential material for several applications, including solar cell devices,[32] catalysts,[33] light-emitting diodes,[34] field-effect transistors,[35] and development of PEC sensors.[36-38]

Poly(D-glucosamine), p-DG, or chitosan, is a biopolymer reported as film-forming materials with interesting characteristics such as biocompatibility and biodegradability.[39] The p-DG chains have plenty of free primary amino groups and hydroxyl groups, whose protonated amino groups stay positively charged under weakly acidic conditions, making the electrostatic self-assembly possible with some species.[40] In this sense, p-DG may have a good capacity for forming films with favorable properties to construct sensors and biosensors.[41,42]

In this work, we report the development of a simple PEC method for the detection and quantification of THBA. Thus, a fluorine-doped tin oxide (FTO) electrode was modified by electrodeposition of CdS covered with a p-DG polymer, and a commercial light-emitting diode (LED) light was used as a power source. The PEC sensor showed good PEC activity and fast response.

Experimental

Reagents and chemicals

All reagents were of analytical grade. Cadmium chloride ($CdCl_2$), sodium thiosulphate ($Na_2S_2O_3$), gallic acid ($C_7H_6O_5$), chitosan ($C_6H_{11}O_4N$), acetic acid (CH_3COOH), boric acid (H_3BO_3), phosphoric acid (H_3PO_4), citric acid ($C_6H_8O_7$), glucose ($C_6H_{12}O_6$), saccharose ($C_{12}H_{22}O_{11}$), catechol ($C_6H_6O_2$), caffeic acid ($C_9H_8O_4$), were acquired from Sigma-Aldrich (St. Louis, USA). Sodium hydroxide (NaOH), ethanol (CH_3CH_2OH), disodium phosphate (Na_2HPO_4) and hydrochloric acid (HCl) were acquired from Isofar - Indústria e Comércio de Produtos Químicos Ltda (Duque de Caxias, RJ, Brazil). The working solutions were daily prepared with water purified in an OS100LXE system from GEHAKA Company (São Paulo, Brazil).

Experimental apparatus

PEC measurements were performed with an Autolab potentiostat/galvanostat model PGSTAT 128N (Metrohm Autolab BV, Utrecht, The Netherlands), controlled by Nova 2.1 program. The electrochemical system was composed of an electrochemical cell with a capacity of 5.0 mL, with input for three electrodes. The working, the reference and the auxiliary electrodes were a fluorine-doped tin oxide (FTO), an Ag/AgCl in saturated KCl and a gold electrode (Au), respectively. The cell was housed inside a box containing a 35 W visible-light LED lamp as a light source during PEC measurements.

The PEC platform FTO and CdS/FTO morphologies were investigated by scanning electron microscopy (SEM). SEM images were obtained using a Quanta 200 FEG from FEI Company (Oregon, United States). Raman measurements of FTO, CdS/FTO, and p-DG-CdS/FTO were performed in a T64000 (Jobin-Yvon/Horiba, Kyoto, Japan) spectrometer equipped with a BX41 (Olympus) microscope, for microanalysis, and a liquid N_2-cooled charge-coupled device (CCD), for signal detection. All spectra were obtained at room temperature, exciting with the 532-nm line of a diode-pumped solid-state laser. Each spectrum was obtained after 3 acquisitions of 60 s each.

Scanning electrochemical microscopy (SECM) images were performed with a Sensolytics base (Bochum, Germany) coupled to a bi-potentiostat/galvanostat, model PGSTAT 128 N, from Sensolytics GmbH (Bochum, Germany). The SECM measurements were performed with the aid of a platinum microelectrode of 25 μm diameter. The SECM images were performed in a three-electrode electrochemical cell assembled on top of the p-DG-CdS/FTO surface. A solution containing 5 mmol L^{-1} $[Fe(CN)_6]^{3-}$ and 0.1 mol L^{-1} KCl was used as an electrolyte. The SECM images were performed biasing the tip at −200 mV *vs.* Ag/AgCl in saturated KCl on the unbiased p-DG-CdS/FTO platform.

Construction of the p-DG/CdS/FTO PEC sensor

Initially, the FTO electrode surface was cleaned by immersing the electrode in ethanol and water to remove any impurities. Then, the FTO electrode was modified with CdS by electrodeposition.[31] Briefly, 5 mL of 0.02 mol L^{-1} $CdCl_2$ aqueous solution containing 0.1 mol L^{-1} $Na_2S_2O_3$ was prepared, and the pH of this plating solution was adjusted to about 2.3. Ten cyclic voltammograms were performed by cycling the potential from − 1.0 V to + 0.6 V at a scan rate of 0.01 V s^{-1} *vs.* Ag/AgCl in saturated KCl for the electrodeposition of CdS on FTO surface to obtain the CdS/FTO. In order to modify the CdS/FTO electrode with

p-DG, a solution containing 1% (mass/volume) of the polymer solubilized in acetic acid aqueous solution was initially prepared. An aliquot of 10 μL of the previously prepared p-DG polymer solution was dropped directly on the modified CdS/FTO substrate (surface area of 1 cm^2). After this step, the electrode was allowed to dry for 30 min to form the p-DG-CdS/FTO PEC platform.

Study of the PEC behavior of the sensor in the presence and absence of gallic acid and optimization of the experimental and operational parameters

The responses of the p-DG-CdS/FTO PEC sensor were evaluated by amperometric measurements in the absence and presence of gallic acid. The effects of the gallic acid on the response of the p-DG-CdS/FTO PEC sensor were evaluated in 0.1 mol L^{-1} phosphate-buffered solution, pH 7.0, biasing the working electrode at 0.0 V *vs*. Ag/AgCl in saturated KCl.

Some experimental conditions and operational parameters that influence the PEC system's sensitivity and response were optimized to obtain a better performance for the proposed p-DG-CdS/FTO sensor. Initially, the effect of the pH of the electrolyte on the response of the photosensor to gallic acid was studied in a pH range of 6.0 to 7.5. After the optimization of pH, the analytical signal of the PEC sensor for acid gallic was also analyzed using four different types of buffer solutions (phosphate (PB), McIlvaine (MCV) and Britton-Robinson (BR)) in a concentration of 0.1 mol L^{-1}. The applied potential effect was also optimized to obtain the highest values of photocurrent with the proposed system. Thus, the photocurrent was monitored under the following applied potentials: –0.3, –0.2, –0.1, 0.0, 0.1, 0.2 and 0.3 V *vs*. Ag/AgCl in saturated KCl under buffer solution and pH-optimized conditions.

Preparation of commercial samples and p-DG-CdS/FTO sensor application

The application of the p-DG-CdS/FTO sensor was performed in commercial samples of tea sachets and wines. The samples were obtained from a local supermarket and prepared by adapting the methodology used in previously published works.[43] Briefly, the infusion of the tea samples was performed by immersing tea sachet samples in 20 mL of boiling water for 6 min. After the samples preparation, 200 μL aliquot of each sample (tea and wine) was added to the electrochemical cell containing the supporting electrolyte and the amperometric measurements were performed under an optimized applied potential (0.0 V *vs.* Ag/AgCl in saturated KCl). The standard addition method was performed by five additions of 10 μL of the standard solution (0.0025 mol L^{-1}) in the electrochemical cell for the samples fortified with 1 μmol L^{-1} of the standard solution. On the other hand, the samples fortified with 5 μmol L^{-1} of the standard solution have received five additions of 10 μL of the standard solution (0.005 mol L^{-1}) in the electrochemical cell.

Analytical characterization of the p-DG-CdS/FTO sensor

After optimizing the experimental and operational parameters, the analytical curve of the p-DG/CdS/FTO sensor for determination of THBA and the limit of detection (LOD) were obtained by amperometry. The accuracy of the developed sensor was evaluated considering the repeatability of ten successive measurements of the photocurrent of the proposed sensor for 10 μmol L^{-1} THBA. The reproducibility for preparing four different sensors, prepared in the same way and on different days, was also evaluated. All measurements were performed under experimental conditions previously optimized for the p-DG-CdS/FTO.

Results and Discussion

Characterization of the materials

In order to characterize the morphology of the fluorine-doped tin oxide substrate (FTO film) modified with cadmium sulfide and compare it with the unmodified FTO surface, scanning electron microscopy images were performed for the electrodeposited CdS films. Figures 1a and 1b show the micrographs of the unmodified and modified FTO, respectively. According to these figures, it can be seen that the film of fluorine-doped tin oxide deposited on the glass slide substrate is composed mainly of crystals of pyramidal shape, while the film of CdS modified FTO presents small particles of nodule aspect. X-ray dispersive energy (EDX) measurements were performed on the substrates of unmodified (Figure 1c) and modified (Figure 1d) FTO. Figure 1c shows the main elements observed in the FTO-containing glass substrate, i.e., Sn, O, F, Si and Sn. Figure 1d shows, in addition to the elements already mentioned in Figure 1c, the presence of S and Cd in a ratio of 1:1, confirming the presence of the cadmium sulfide film. The presence of carbon, seen in the spectra of Figures 1c and 1d, is typical of pure FTO, mainly caused by contamination due to ambient air.[44]

In addition, Figure 1e shows the Raman spectra for the unmodified FTO substrate (black spectrum) and modified one with CdS (red spectrum) and with CdS and p-DG

(blue spectrum). The red spectrum of Figure 1e shows two peaks located at approximately 300 and 602 cm^{-1} that are directly related to the active modes LO and 2LO (first and second-order longitudinal optical modes), respectively, of CdS, confirming the presence of the CdS deposited on the surface of the FTO.[45] On the other hand, for the complete material (blue spectrum) in the presence of p-DG, it is possible to observe the appearance of bands that evidence the presence of the polymer on the surface of the CdS/FTO electrode.

The peaks at 1255 and 1370 cm^{-1} can be associated with the combination of different modes of the polymer, i.e., δ(OH...O) + ν(C–C) + ν(C–O) + δ(CH) + $\rho(CH_2)$ for the first peak and $\delta(CH_2)$ + δ(CH) + δ(OH) + $\nu(\varphi)$ for the second one.[46] Other peaks can be seen at 430, 462 and 1057 cm^{-1}, which can be attributed to flexion modes outside the γ(O–H) plane and flexion vibrations in the δ(C–H) plane, respectively.[47-49] The black spectrum of Figure 1e shows only the bands corresponding to the FTO's vibrational modes.[50]

In order to evaluate the spatial photoactivity of the PEC platform, SECM images of the platform under dark and light conditions were performed. Figures 2a and 2b show SECM images that were taken to assess the effect

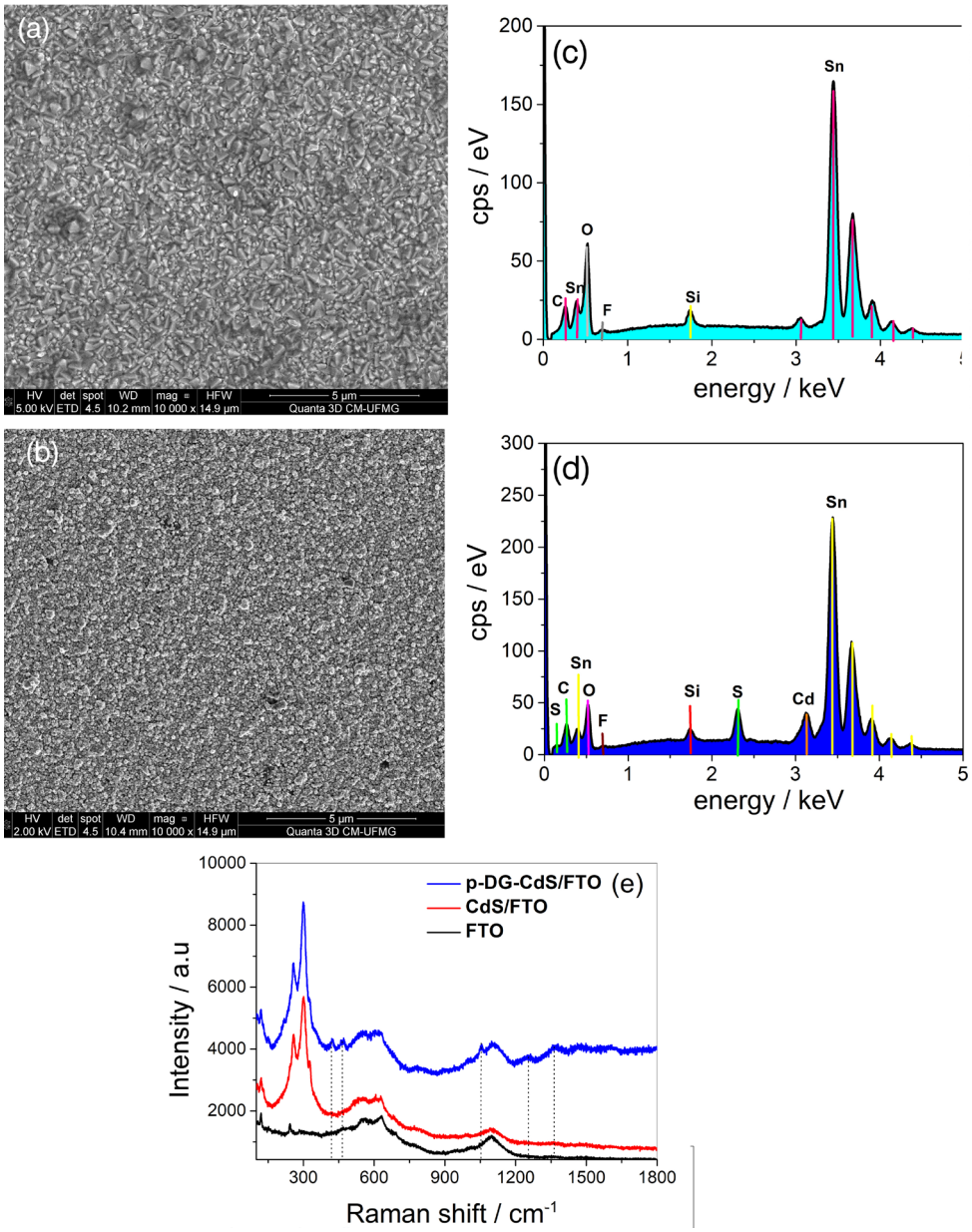

Figure 1. SEM measurements for the unmodified FTO electrode (a) and the CdS modified FTO electrode (b). EDX spectra are referring to (a) and (b), respectively (c) and (d); Raman spectra referring to the FTO electrode modified with CdS/p-DG (blue spectrum), the FTO electrode modified only with CdS (red spectrum) and the FTO surface (black spectrum) (e).

of visible LED light on the ability of the p-DG-CdS/FTO PEC platform to generate spatially separated electrons and holes at the sensor surface.

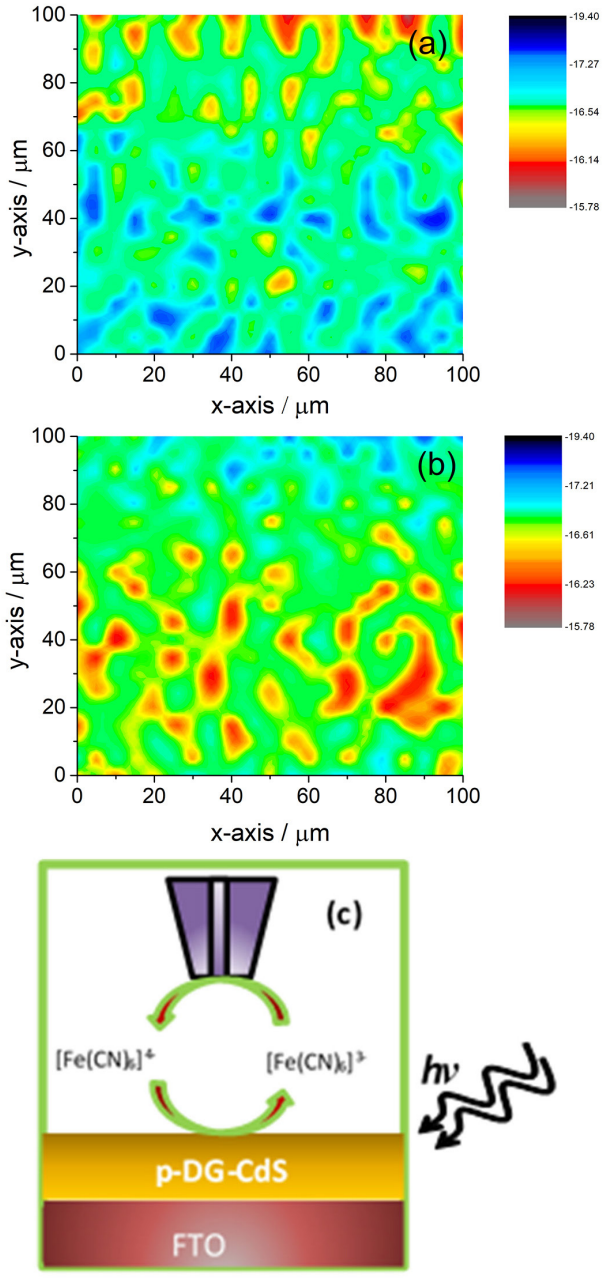

Figure 2. SECM images of p-DG-CdS/FTO under visible LED light condition (a) and absence of light (b) obtained in 0.1 mol L^{-1} KCl aqueous solution containing 5 mmol L^{-1} $[Fe(CN)_6]^{3-}$. (c) Schematic diagram of the SECM experiments. The tip was biased at −200 mV *vs.* Ag/AgCl in saturated KCl.

As can be seen, large areas of blue color appear in the colormap obtained under light (Figure 2a), while areas of red color appear in greater quantity in the colormap obtained in the absence of light (Figure 2b). Therefore, the feedback currents obtained in the probe in the absence of light (Figure 2b) were lower than those obtained under light conditions (Figure 2a). Thus, SECM images show that the p-DG-CdS/FTO PEC sensor is strongly spatially sensitive to the presence of light. The photogenerated holes can collect the ferrocyanide species generated at the tip, increasing the feedback current (Figure 2c).

For the electrochemical characterization of CdS/FTO and p-DG-CdS/FTO, electrochemical impedance spectroscopy (EIS) experiments were performed using a 5 mL electrochemical cell using a conventional three-electrode system. Nyquist spectra were performed in a 0.1 mol L^{-1} KCl containing 5 mmol L^{-1} $K_3[Fe(CN)_6]$ in the absence and presence of light in a frequency ranging from 10^{-1} to 10^4 Hz. Figures 3a and 3b show the impedance spectra for the CdS/FTO PEC platform in the presence of the p-DG polymer and the absence of the polymer, respectively. In addition, these figures also show the responses of the p-DG-CdS/FTO and CdS/FTO platforms in the absence (black spectrum) and the presence of visible light (red spectrum).

As shown in Figure 3, the p-DG-CdS/FTO presents a smaller semicircle diameter in the presence and absence of light when compared to CdS/FTO. In order to evaluate the charge transfer resistance of each material in the presence and absence of light the Nyquist plots were fitted by using a Randles equivalent circuit.[51] The p-DG-CdS/FTO presented a charge transfer resistance (R_{ct}) under absence of light 4.25 kΩ while the CdS/FTO presented a R_{ct} of 9.32 kΩ. In addition, the charge transfer resistance of p-DG-CdS/FTO (R_{ct} = 1.69 kΩ) in the presence of light was lower than that observed for CdS/FTO (R_{ct} = 2.90 kΩ) also in the presence of light. Therefore, the presence of the chitosan has improved the charge transfer resistance of the PEC system in the absence and presence of light. The lower charge transfer resistance in the presence of light can be due to the intrinsic value of pK_a of chitosan that is about 6.3.[52] Thus, some positive charges associated to residual protonated amino groups in chitosan can perform an electrostatic interaction with the ferricyanide since the pK_a of the chitosan is close to pH of the solution.[53] In this sense, this behavior suggests that the presence of the polymer contribute to the reduction of the resistance to the charge transfer through the interface.

In addition, the EIS also shows that, when the electrodes are in the presence of light, there is a significant decrease in the charge transfer resistance compared to the spectra obtained in the absence of light, showing the strong effect of light on the electrode surfaces. This result suggests that the semiconductor can absorbs photons from light to generate charge carriers (electron-hole pairs) in the conduction and valence bands. Then, the photogenerated electrons can flow

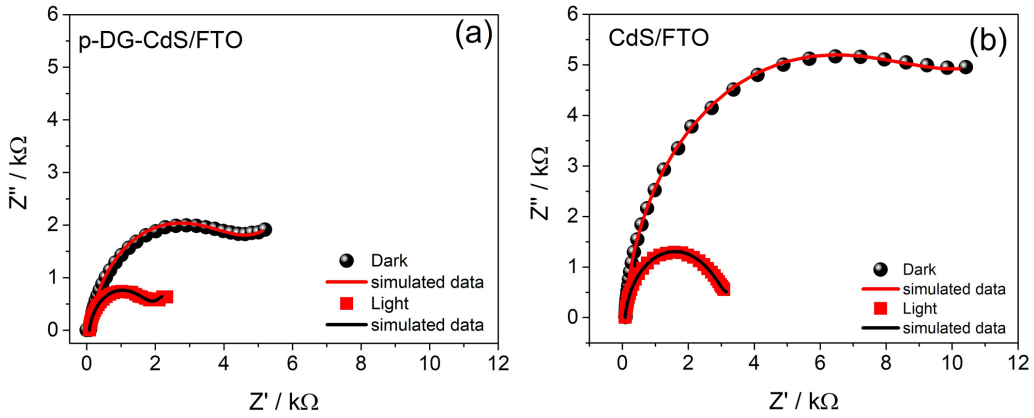

Figure 3. (a) Nyquist plots performed in solution 0.1 mol L^{-1} KCl containing 5 mmol L^{-1} $[Fe(CN)_6]^{3-}$ for the FTO modified with p-DG/CdS (p-DG/CdS/FTO) under dark (black circles) and visible LED light condition (red squares). (b) Nyquist plots for the FTO modified with CdS (CdS/FTO), recorded in 0.1 mol L^{-1} KCl containing 5 mmol L^{-1} $[Fe(CN)_6]^{3-}$ under dark (black circles) and visible LED light condition (red squares). The simulated data are presented as full line.

to the external circuit while in the dark a higher electron accumulation in the electrode can result in a higher charge transfer resistance.[54,55]

Study of the electrochemical behavior and the best experimental conditions for the determination of THBA

In order to evaluate the electrochemical response of the p-DG-CdS/FTO, CdS/FTO, and unmodified FTO platforms under the incidence of light from a LED lamp, amperograms for each material were obtained in 0.1 mol L^{-1} of PB, pH 7.0, under an applied potential of 0.3 V *vs*. Ag/AgCl in saturated KCl. Figure 4a show the amperograms of the p-DG-CdS/FTO, CdS/FTO, and unmodified FTO in absence and presence of 20 μmol L^{-1} THBA. Under incidence of light, electrons can leave the valence band being promoted to the conduction band of the PEC platforms to produce electron/hole pairs (e^-/h^+). In Figure 4a the results show that the p-DG-CdS/FTO platform presented a larger photocurrent in comparison to the obtained for the CdS/FTO and FTO unmodified electrodes in absence or presence of THBA. These results suggest that when the visible light impinges the surface of p-DG-CdS/FTO, the electron in the valence band can receive sufficient energy to be promoted from the valence band to the conduction band. The photogeneration of carriers can be probably more efficient due to the narrow band gap of CdS and the presence of polymer on the electrode surface, which can probably contribute to the increase of CdS photostability and efficiency of carrier separation in comparison to the CdS/FTO and FTO unmodified electrodes. In addition, it can also be observed that the presence of the analyte on the electrodic surfaces decreases the photocurrent of the p-DG-CdS/FTO and CdS/FTO, and of the unmodified electrode promoting a decrease of the photocurrent of the system, which can be monitored by the variation of the current ($\Delta I = I_0 - I$, where I_0 and I are the photocurrents in the absence and presence of the analyte, respectively). Therefore, the p-DG-CdS/FTO PEC sensor presents a higher capability to the PEC determination of THBA.

Figure 4b shows the amperometric behavior of the p-DG/CdS/FTO platform in the absence (black amperogram) and the presence of different concentrations of THBA: 20 μmol L^{-1} (red amperogram); 30 μmol L^{-1} (blue amperogram); 60 μmol L^{-1} (pink amperogram), and 200 μmol L^{-1} (green amperogram).

As shown in the amperograms in Figure 4b, the photocurrent of the sensor decreases as the THBA concentration increases. This fact may be related to the ability of the analyte to inhibit the water oxidation with the p-DG-CdS/FTO electrode (Figure 4b). According to the proposed mechanism to the response of the PEC platform for analyte presented in Figure 4c, the surface of the CdS can interact with an enediol ligand like THBA to attract electrons from the CdS conduction band. This interaction can result in a donor to the acceptor transfer of electrons at the interface. Thus, when THBA and CdS interact with each other, electron/charge transfer occurs from CdS to THBA, and this phenomenon can result in non-radioactive recombination.[56,57] In addition, the amine groups of chitosan and carboxylic group of THBA can favor the interaction between the analyte and the platform, improving the inhibition of the response of the PEC platform.

It is also observed that, when the photocurrent is plotted as a function of the logarithm of the concentration (inset of Figure 4b), a linear correlation is obtained, indicating that it is possible to perform the quantification of the antioxidant through the monitoring of the analytical signal. This result suggests that it is possible to perform the determination of the analyte with a good variation of the analytical signal. In this sense, in order to evaluate the best experimental and

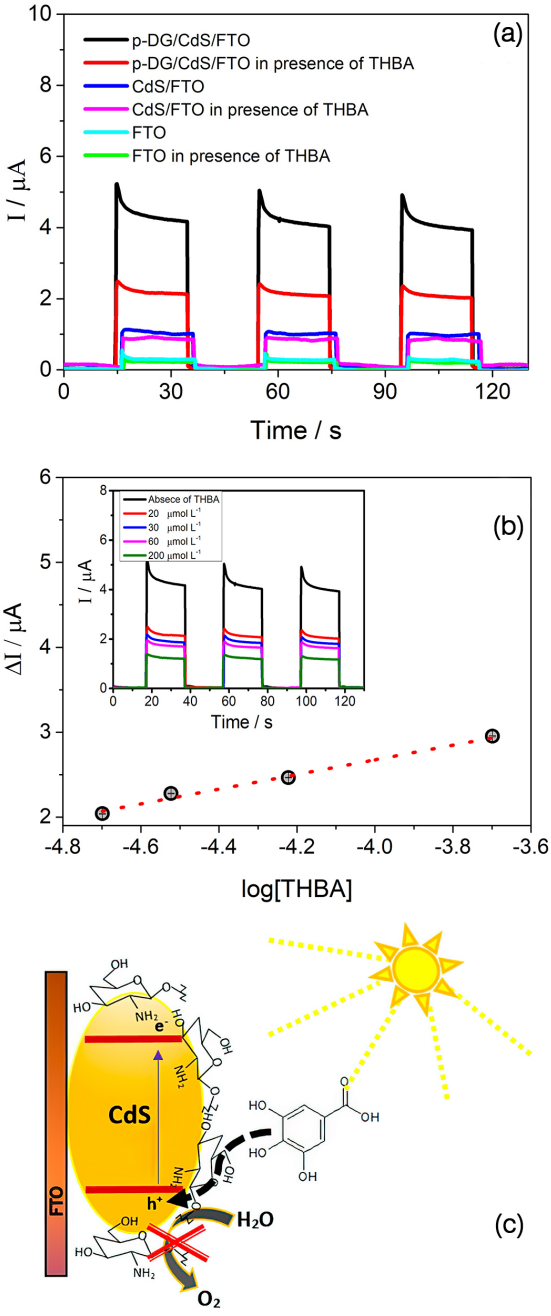

Figure 4. (a) Amperograms of the p-DG-CdS/FTO PEC sensor in absence (black amperogram) and presence (red amperogram) of 20 µmol L^{-1} THBA; CdS/FTO sensor in absence (blue amperogram) and presence of 20 µmol L^{-1} THBA (pink amperogram), unmodified FTO in absence (cyan amperogram) and presence of 20 µmol L^{-1} THBA (green amperogram). (b) Amperograms of the p-DG-CdS/FTO PEC sensor in the absence and presence of different analyte concentrations (20; 30; 60 and 200 µmol L^{-1}), pH 7.0. Inset of Figure 4b: plot of the variation of the photocurrent *vs.* the [THBA]. Experiments were performed on 0.1 mol L^{-1} PB. E_{appl} = 0.3 V *vs.* Ag/AgCl in saturated KCl. (c) Schematic representation of the proposed mechanism for the detection of THBA with p-DG-CdS/FTO PEC sensor.

operational conditions to found the higher PEC response for the detection and quantification of the analyte, some variables were investigated.

The effects of the experimental and operational parameters on the response of the modified electrode to the analyte were investigated by evaluating the pH of the medium, type of buffer solution and applied potential. Figure 5a shows the plot of the photocurrent as a function of pH (pH 6.0, 6.5, 7.0 and 7.5) in order to show the effect of the influence of the concentration of hydrogen ions in the medium on the sensor response. For this study, the PB solution was used at a concentration of 0.1 mol L^{-1}. As can be seen in Figure 4b, the photocurrents of the p-DG-CdS/FTO PEC sensor increased from pH 6.0 to 7.0 and decreased significantly after that pH. Thus, for the other studies, it was established to use an electrolyte solution with pH 7.0.

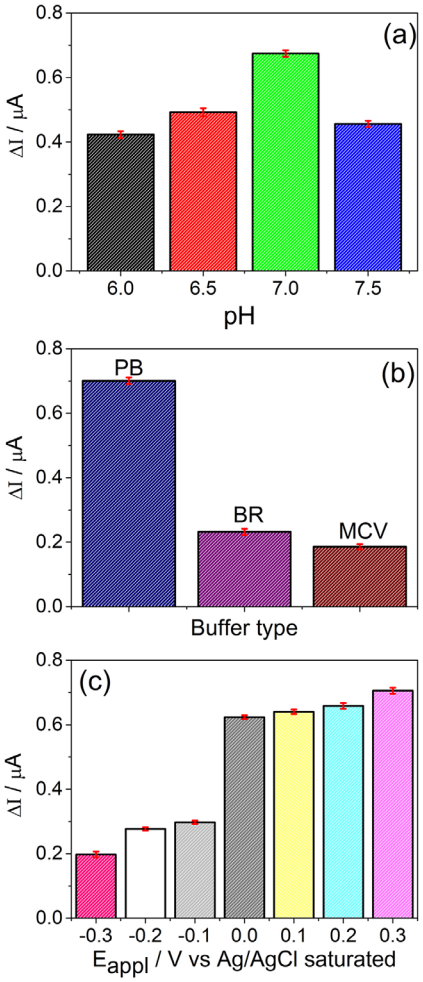

Figure 5. (a) Influence of pH (6.0; 6.5; 7.0 and 7.5) on the PEC response of the sensor in 0.1 mol L^{-1}. E_{appl} = 0.3 V *vs.* Ag/AgCl in saturated KCl; (b) Influence of the buffer solution (0.1 mol L^{-1}) on the PEC response of the sensor. E_{appl} = 0.3 V. (c) Influence of the applied potential (E_{appl}) on the response of the PEC sensor in 0.1 mol L^{-1} PB [THBA] = 2 µmol L^{-1}.

Subsequently, the influence of the type of buffer solution on the sensor response was evaluated. In this sense, the effects of buffer on the response of the platform

to the analyte were evaluated in phosphate, McIlvaine (MV) buffer and Britton-Robinson (BR) buffer solution. Figure 5b shows the PEC responses of the platform to the analyte in these different types of buffer solutions in a concentration of 0.1 mol L^{-1}. It was observed that the highest values of photocurrent shift were obtained in PB, while, for the other electrolytes, the photocurrents showed lower values in terms of photocurrent variation. This result suggests that, in PB, the antioxidant molecule is able to diffuse much more easily from the bulk of the solution to the surface of the photoelectrode p-DG-CdS/FTO. Then, the phosphate buffer solution, in a concentration of 0.1 mol L^{-1} (pH 7.0), was employed for further studies.

Finally, to establish the most suitable potential for obtaining the analyte response with greater sensitivity while biasing the electrode at a low potential, the effects of the applied potential (E_{appl}) on the working electrode (Figure 5c) were evaluated. For this purpose, the photoelectrode was biased at the following potentials: –0.3, –0.2, –0.1, 0.0, 0.1, 0.2 and 0.3 V *vs.* Ag/AgCl in saturated KCl. Figure 5c shows the results obtained for these different applied potentials in 0.1 mol L^{-1} PB containing 2 µmol L^{-1} THBA. As can be seen, it is observed that the photocurrent variation (decrease of photocurrent) between the response of the photosensor p-DG-CdS/FTO increases significantly from potential –0.3 to 0.0 V, and after 0.0 V, the effect of the potential applied on the PEC platform was not so significant. These results suggest that it is enough to use a potential of 0.0 V to obtain a high photocurrent variation value. Under these conditions, greater sensitivity to the system is achieved while maintaining low biasing conditions, making it possible to determine the analyte even at very low concentrations consuming a minimum of energy. In addition, the applied potential is an important parameter that directly influences the analytical performance of the sensor. Thus, it is possible to significantly reduce or eliminate the possible influence of interfering species on electrocatalytic processes that occur at a potential of the order of 0.0 V *vs.* Ag/AgCl in saturated KCl. In this sense, an applied potential of 0.0 V was chosen to construct the analytical curve for the determination of the antioxidant.

Analytical characterization

After optimizing the experimental conditions for the determination of THBA in 0.1 mol L^{-1} of PB pH 7.0, an analytical curve was constructed under an applied potential of 0.0 V after successive additions of the standard solution in the electrochemical cell. Thus, Figure 6 shows the amperograms obtained at different concentrations (Figure 6a) and the plot of photocurrent as a function of THBA concentration obtained from Figure 6a (Figure 6b). According to the results obtained in Figure 6b, the variation of the photocurrent of the p-DG-CdS/FTO PEC sensor, ΔI, increases with the logarithm of concentration of THBA. In this sense, it was possible to observe a linear working range from 0.2 to 500 µmol L^{-1} for THBA, with a correlation coefficient of 0.998 (for n = 10). The linear regression equation is expressed as: ΔI (µA) = 5.53 + 0.79 log [THBA] (mol L^{-1}).

The lowest detectable concentration was 0.1 µmol L^{-1} taking into account a signal-to-noise ratio of 3 (S/N = 3). Based on these results, it can be inferred that the proposed method presented a good limit of detection, indicating that this method is an excellent alternative for the determination of THBQ. The linear response of the sensor was compared to other works reported in the literature for the detection of THBA (Table 1).[7,12-16,18,20,22,58-62] It is observed that, concerning the techniques presented in Table 1, the proposed method showed satisfactory results, since it can be used successfully in the determination of THBA. It is

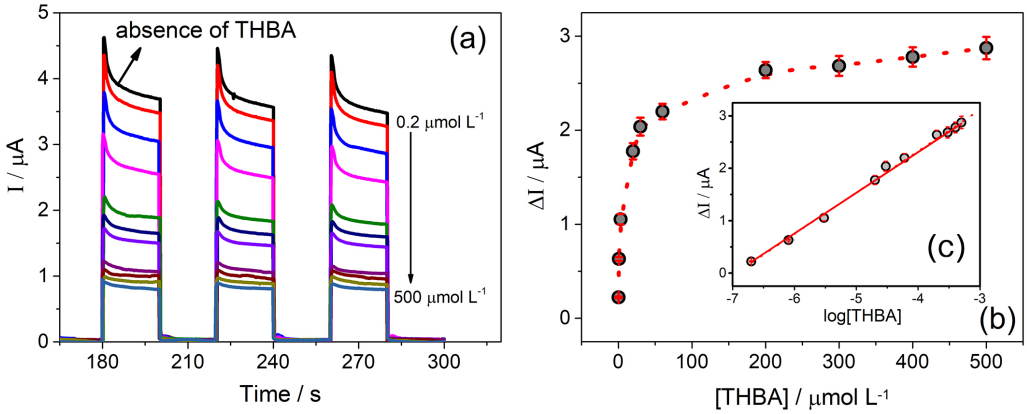

Figure 6. (a) Amperograms of the p-DG/CdS/FTO photosensor in the absence and presence of different concentrations of the analyte (0.2 to 500 µmol L^{-1}) in 0.1 mol L^{-1} PB, pH 7.0; (b) plot of the variation of the photocurrent ΔI *vs.* [THBA]; (c) analytical curve obtained from the variation of photocurrent ΔI *vs.* log [THBA]. E_{appl} = 0.0 V *vs.* Ag/AgCl in saturated KCl.

Table 1. Comparison of analytical characteristics of different methods reported for the determination of THBA

Method	LOD / (μmol L^{-1})	Linear range / (μmol L^{-1})	Reference
Amperometry	0.16	1-100	7
Spectrophotometry	0.353	0-41	12
FIA-spectrophotometry	0.476	0.589-205.7	14
FIA-chemiluminescence	2.94×10^{-3}	4.70×10^{-3}-5.87×10^{-1}	15
Spectrophotometry	0.016	8.82×10^{-2}-3.53×10	16
Chemiluminescence	6.1×10^{-2}	1×10^{2}-1×10^{-1}	18
SWV	0.0867	0.51-46.40	20
DPV	0.025	0.22-55	22
UHPLC-MS	0.118	0.118-59	58
LC-MS/MS	5.9×10^{-3}	11.8×10^{-3}-59×10^{-1}	13
DPV	0.15	0.2-5.0 5.0-100	59
DPV	1.2×10^{-3}	0.08-20	60
Fluorescence	3.30×10^{-3}	3.53-74.06	61
DPV	0.15	1-100	62
PEC	0.1[a]	0.2-500	this work

[a]The LOD was determined experimentally. FIA: flow injection analysis; SWV: square wave voltammetry; DPV: differential pulse voltammetry; UHPLC-MS: ultra-high performance liquid chromatography; LC-MS/MS: liquid chromatography mass spectrometry; PEC: photoelectrochemical.

also important to emphasize that the proposed method does not involve co-precipitation steps, flow injection, and it does not require large amounts of samples, being easy to prepare and operate.

In order to evaluate the repeatability of the response of the proposed PEC sensor, successive measurements were performed in a time interval of about 500 s in the presence of 50 μmol L^{-1} THBA in 0.1 mol L^{-1} PB (pH 7.0) and at an applied potential of 0.0 V *vs.* Ag/AgCl in saturated KCl. The relative standard deviation (RSD) between the first and last photocurrent was about 6.8% and the RSD for all photocurrents was about 4.0% (Figure 7a). According to the results, it was observed that the proposed sensor provided a satisfactory RSD value for measurements performed on the same working day, suggesting that the sensor has good repeatability. Additionally, four electrodes were modified under the same conditions at different working days in the presence of 50 μmol L^{-1} THBA in order to also evaluate the reproducibility in the preparation of these sensors (Figure 7b). The RSD for the mean values of the photocurrents obtained for each electrode prepared at different days were 4.5, 2.8, 2.6 and 3.6%, respectively. Based on these results, it was possible to calculate an average RSD value lower than 5.0% for the photocurrent measurements obtained at different working days. Finally, it can be observed that the proposed PEC sensor presented good precision in terms of repeatability and reproducibility. The prepared platforms were stored at room temperature and kept in the absence of light.

Interferent study

In order to evaluate the selectivity of the p-DG-CdS/FTO PEC sensor, the influence of other compounds that may be present in samples containing THBA, such as chlorogenic acid, saccharose, glucose, and catechol, was investigated. Thus, this study was carried out keeping the sensor in the presence of 50 μmol L^{-1} of THBA and possible interferents species (50 μmol L^{-1}).

The results are shown in Figure 7c, in which it is observed that there was no significant change in the values of THBA photocurrents compared to the values for the other interferents. It is also observed that the percentage values found between the THBA photocurrent and the interfering compounds are very close, with values below 5%. Therefore, these results demonstrate that the determination of this antioxidant with the proposed method is not significantly influenced by the response of the tested interferents, indicating a good selectivity for the determination of THBA in the presence of these species.

Determination of THBA in wine and tea samples and analyte addition and recovery studies

Finally, to evaluate the application and efficiency of the proposed method in real samples, it was tested in two different samples (wine and tea samples). The determination of THBA in each sample was performed under optimized experimental conditions.

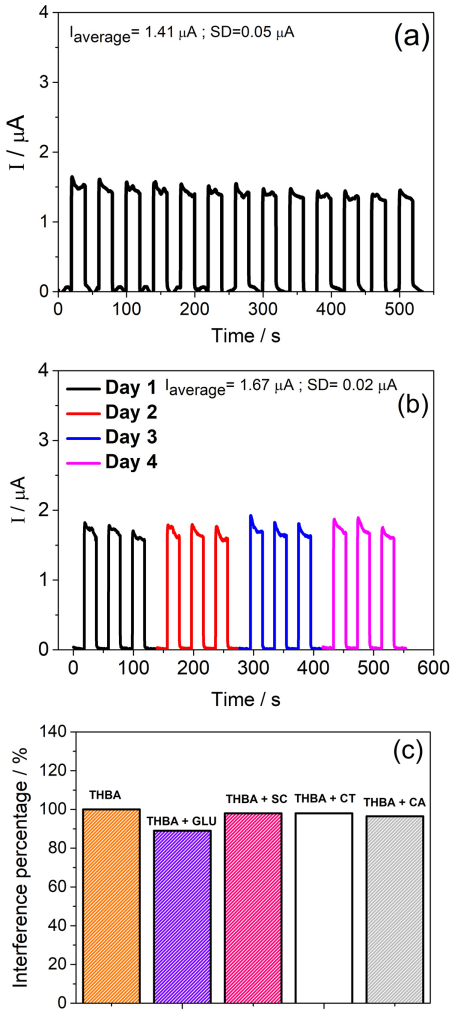

Figure 7. Evaluation of repeatability of measurements performed on the same day (a) and different days (b). The measurements were performed with the p-DG-CdS/FTO PEC sensor in 0.1 mol L^{-1} phosphate-buffered solution, containing 50 μmol L^{-1} THBA. E_{appl} = 0.0 V *vs.* Ag/AgCl in saturated KCl. (c) Influence of possible interferences on the photocurrent of THBA, THBA + glucose (GLU), THBA + saccharose (SC), THBA + catechol (CT) and THBA + caffeic acid (CA). Experiments were carried out in 0.1 mol L^{-1} PB, pH 7.0. E_{appl} = 0.0 V *vs.* Ag/AgCl in saturated KCl.

Thus, Table 2 presents the THBA concentrations for the samples and their respective analyte recovery values. It is observed that the percentage recovery obtained after the addition of known concentrations of THBA in the samples varied between 95.88 and 101.72%. These values indicate that the method can be applied to these samples without significant interference from the matrix. Furthermore, it is observed that the proposed method presented an excellent accuracy and efficiency of the sensor for the determination of THBA in the studied samples.

Conclusions

This work describes the development of a PEC platform p-DG-CdS/FTO as an alternative for the determination of 3,4,5-trihidroxybenzoic acid (THBA) in samples of wine and tea. The optimization of the experimental conditions resulted in figures of merit similar to those observed to some other methods described in the literature. In addition, the proposed method does not involve co-precipitation steps, flow injection, and it does not require large amounts of samples, being easy to prepare and operate. Thus, this PEC sensor showed good repeatability, evaluated in terms of relative standard deviations and appreciable percentage of recovery for the samples. Therefore, p-DG-CdS/FTO PEC sensor is a viable alternative for the detection of THBA.

Acknowledgments

The authors are grateful to FAPEMA (INFRA-03186/18; UNIVERSAL-01057/19; UNIVERSAL-01194/17), CNPq (308204/2018-2; 309828/2020-1), Instituto Nacional de Ciência e Tecnologia em Bioanalítica (465389/2014-7), and FINEP for financial support.

Table 2. Recovery values of THBA obtained for two samples (number of replicates = 3)

Sample	[THBA] added / (μmol L^{-1})	[THBA] expected / (μmol L^{-1})	[THBA] found[a] / (μmol L^{-1})	Recovery / %
Wine A	0	–	0.64 (± 0.07)	–
	1.00	1.64	1.60 (± 0.10)	97.56
	5.00	5.64	5.60 (± 0.22)	99.29
Wine B	0	–	1.16 (± 0.03)	–
	1.00	1.16	1.18 (± 0.07)	101.72
	5.00	5.16	5.09 (± 0.06)	98.64
Black tea	0	–	0.70 (± 0.05)	–
	1.00	1.70	1.63 (± 0.12)	95.88
	5.00	5.70	5.62 (± 0.18)	98.60
Green tea	0	–	0.37 (± 0.01)	–
	1.00	1.37	1.32 (± 0.05)	96.35
	5.00	5.37	5.20 (± 0.14)	96.83

[a]Values determined in the electrochemical cell.

References

1. Stavrou, I. J.; Christou, A.; Kapnissi-Christodoulou, C. P.; *Food Chem*. **2018**, *269*, 355.
2. Arribas, A. S.; Moreno, M.; Gonzaléz, L.; Blázquez, N.; Bermejo, E.; Zapardiel, A.; Chicharro, M.; *J. Electroanal. Chem*. **2020**, *857*, 113750.
3. Xiong, C.; Wang, Y.; Qu, H.; Zhang, L.; Qiu, L.; Chen, W.; Yan, F.; Zheng, L.; *Sens. Actuators, B* **2017**, *246*, 235.
4. Zhao, M. T.; Liu, Z. Y.; Li, A.; Zhao, G. H.; Xie, H. K.; Zhou, D. Y.; Wang, T.; *LWT-Food Sci. Technol*. **2021**, *139*, 110551.
5. Badea, M.; di Modugno, F.; Floroian, L.; Tit, D. M.; Restani, P.; Bungau, S.; Iovan, C.; Badea, G. E.; Aleya, L.; *Sci. Total Environ*. **2019**, *672*, 129.
6. Nazari, F.; Ghoreishi, S. M.; Khoobi, A.; *Int. J. Biol. Macromol*. **2020**, *160*, 456.
7. Madhusudhana; Manasa, G.; Bhakta, A. K.; Mekhalif, Z.; Mascarenhas, R. J.; *Mater. Sci. Energy Technol*. **2020**, *3*, 174.
8. Mikoiłajczak, N.; Tańska, M.; Ogrodowska, D.; *Trends Food Sci. Technol.* **2021**, *113*, 110.
9. Tian, W.; Chen, G.; Zhang, G.; Wang, D.; Tilley, M.; Li, Y.; *Food Chem*. **2021**, *344*, 128633.
10. Ao, J.; Zhang, Q.; Tang, W.; Yuan, T.; Zhang, J.; *Chemosphere* **2021**, *278*, 130494.
11. Lima, F. M. R.; Silva, S. M.; Freires, A. S.; Goulart, M. O. F.; Damos, F. S.; Luz, R. C. S.; *J. Solid State Electrochem.* **2019**, *23*, 725.
12. Zaripour, M.; Zare-Shahabadi, V.; Jahromi, H. J.; *Spectrochim. Acta, Part A* **2019**, *222*, 117197.
13. Seo, S. Y.; Kang, W.; *J. Pharm. Biomed. Anal.* **2016**, *131*, 103.
14. Phakthong, W.; Liawruangrath, B.; Liawruangrath, S.; *Talanta* **2014**, *130*, 577.
15. Li, S.; Sun, H.; Wang, D.; Qian, L.; Zhu, Y.; Tao, S.; *Chin. J. Chem.* **2012**, *30*, 837.
16. Pooralhossini, J.; Ghaedi, M.; Zanjanchi, M. A.; Asafaram, A.; *Ultrason. Sonochem.* **2017**, *34*, 692.
17. Qader, H. A.; Fakhre, N. A.; Dikran, S. B.; Hamad, H. H.; *Zanco J. Pure Appl. Sci*. **2019**, *31*, 60.
18. Shah, S. N. A.; Li, H.; Lin, J. M.; *Talanta* **2016**, *153*, 23.
19. Koçak, Ç. C.; Karabiberoğlu, Ş. U.; Dursun, Z.; *J. Electroanal. Chem*. **2019**, *853*, 113552.
20. Węgiel, J.; Burnat, B.; Skrzypek, S.; *Diamond Relat. Mater*. **2018**, *88*, 137.
21. Ziyatdinova, G.; Kozlova, E.; Budnikov, H.; *J. Electroanal. Chem*. **2018**, *821*, 73.
22. Shahamirifard, S. A.; Ghaedi, M.; Razmi, Z.; Hajati, S.; *Biosens. Bioelectron.* **2018**, *114*, 30.
23. Sousa, C. S.; Lima, K. C. M. S.; Botelho, C. N.; Pereira, N. M.; Fernandes, R. N.; Silva, G. G.; Damos, F. S.; Luz, R. C. S.; *J. Solid State Electrochem.* **2020**, *24*, 1715.
24. Freires, A. S.; Botelho, C. N.; Silva, S. M.; Goulart, M. O. F.; Damos, F. S.; Luz, R. C. S.; *Microchem. J.* **2020**, *159*, 105487.
25. Monteiro, T. O.; Santos, C. C.; Prado, T. M.; Damos, F. S.; Luz, R. C. S.; Fatibello-Filho, O.; *J. Solid State Electrochem*. **2020**, *24*, 1801.
26. Peralta-Zamora, P.; *J. Braz. Chem. Soc*. **2010**, *21*, 1621.
27. Zhang, K.; Lv, S.; Lu, M.; Tang, D.; *Biosens. Bioelectron.* **2018**, *117*, 590.
28. Freires, A. S.; Lima, F. M. R.; Yotsumoto-Neto, S.; Silva, S. M.; Damos, F. S.; Luz, R. C. S.; *Microchem. J.* **2018**, *139*, 18.
29. Wang, J.; Zhang, K.; Xu, H.; Yan, B.; Gao, F.; Shi, Y.; Du, Y.; *Sens. Actuators, B* **2018**, *276*, 322.
30. Abdullah, A. M. N. K.; Majeed, K. M.; Ali, S. M.; *Int. J. Metall. Met*. **2020**, *5*, 5.
31. Yotsumoto Neto, S.; Souto, D. E. P.; Andrade, H. M.; Luz, R. C. S.; Kubota, L. T.; Damos, F. S.; *Sens. Actuators, B* **2018**, *256*, 682.
32. Kang, Y.; Kim, D.; *Sol. Energy Mater. Sol. Cells* **2006**, *90*, 166.
33. Zhao, Z.; Cheng, D. G.; Chen, F.; Zhan, X.; *Int. J. Hydrogen Energy* **2020**, *45*, 33532.
34. Zhang, Y.; Zhang, F.; Wang, H.; Wang, L.; Wang, F.; Lin, Q.; Shen, H.; Li, L. S.; *Opt. Express* **2019**, *27*, 7935.
35. Mereu, B.; Sarau, G.; Pentia, E.; Draghici, V.; Lisca, M.; Botila, T.; Pintilie, L.; *Mater. Sci. Eng., B* **2004**, *109*, 260.
36. Gao, B.; Liang, Z.; Han, D.; Han, F.; Fu, W.; Wang, W.; Liu, Z.; Niu, L.; *Talanta* **2021**, *224*, 121924.
37. Zhong, Y.; Yang, S.; Zhang, S.; Cai, X.; Gao, Q.; Yu, X.; Xu, Y.; Zhou, X.; Peng, F.; Fang, Y.; *J. Power Sources* **2019**, *430*, 32.
38. Yu, L. D.; Wang, Y. N.; Zhang, X. Y.; Li, N. B.; Luo, H. Q.; *Sens. Actuators, B* **2021**, *340*, 129988.
39. Liu, J.; Pu, H.; Liu, S.; Kan, J.; Jin, C.; *Carbohydr. Polym*. **2017**, *174*, 999.
40. Huang, F.; Lin, X.; Cheng, C.; Chen, P.; *Appl. Surf. Sci*. **2012**, *258*, 7359.
41. Zouaoui, F.; Bourouina-Bacha, S.; Bourouina, M.; Jaffrezic-Renault, N.; Zine, N.; Errachid, A.; *TrAC, Trends Anal. Chem.* **2020**, *130*, 115982.
42. Midya, L.; Patra, A. S.; Banerjee, C.; Panda, A. B.; Pal, S.; *J. Hazard. Mater.* **2019**, *369*, 398.
43. Botelho, C. N.; Pereira, N. M.; Silva, G. G.; Menezes, A. S.; Bezerra, C. W. B.; Damos, F. S.; Luz, R. C. S.; *Anal. Methods* **2019**, *11*, 4775.
44. Postek, M. T.; *Scanning* **2006**, *18*, 269.
45. Cai, L.; Du, Y.; Guan, X.; Shen, S.; *Chin. Chem. Lett*. **2019**, *30*, 2363.
46. Eddya, M.; Tbib, B.; El-Hami, K.; *Heliyon* **2020**, *6*, e03486.
47. Ren, X. D.; Liu, Q. S.; Feng, H.; Yin, X. Y.; *Appl. Mech. Mater*. **2014**, *665*, 367.
48. Zając, A.; Hanuza, J.; Wandas, M.; Dymińska, L.; *Spectrochim. Acta, Part A* **2015**, *134*, 114.

49. Usman, F.; Dennis, J. O.; Seong, K. C.; Ahmed, A. Y.; Meriaudeau, F.; Ayodele, O. B.; Tobi, A. R.; Rabih, A. A. S.; Yar, A.; *Results Phys*. **2019**, *15*, 102690.
50. Suresh, S.; Deepak, T. G.; Ni, C.; Sreekala, C. N. O.; Satyanarayana, M.; Nair, A. S.; Pillai, V. P.; Pillai M.; *New J. Chem*. **2016**, *40*, 6228.
51. Zouaoui, F.; Bourouina-Bacha, S.; Bourouina, M.; Abroa-Nemeir, I.; Halima, H. B.; Gallardo-Gonzalez, J.; El Hassani, N. E. A.; Alcacer, A.; Bausells, J.; Jaffrezic-Renault, N.; Zine, N.; Errachid, A.; *Sens. Actuators, B* **2020**, *309*, 127753.
52. Zhang, Y.; Li, Y.; Wu, W.; Jiang, Y.; Hu, B.; *Biosens. Bioelectron*. **2014**, *60*, 271.
53. Zangmeister, R. A.; Park, J. J.; Rubloff, G. W.; Tarlov, M. J.; *Electrochim. Acta* **2006**, *51*, 5324.
54. Lopes, T.; Andrade, L.; Ribeiro, H. A.; Mendes, A.; *Int. J. Hydrogen Energy* **2010**, *35*, 11601.
55. Wang, Y.; Chu, W.; Wang, S.; Li, Z.; Zeng, Y.; Yan, S.; Sun, Y.; *ACS Appl. Mater. Interfaces* **2014**, *6*, 20197.
56. Singh, S.; Garg, S.; Chahal, J.; Raheja, K.; Singh, D.; Singla, M. L.; *Nanotechnology* **2013**, *24*, 115602.
57. Cody, C. A.; Brook, B. G.; Abele, B.; *Sol. Energy Mater*. **1982**, *8*, 231.
58. Sun, Z.; Zhao, L.; Zuo, L.; Qi, C.; Zhao, P.; Hou, X.; *J. Chromatogr. B: Biomed. Sci. Appl.* **2014**, *958*, 55.
59. Liu, H.; Hassan, M.; Bo, X.; Guo, L.; *J. Electroanal. Chem.* **2019**, *849*, 113378.
60. Chen, M.; *Int. J. Electrochem. Sci*. **2019**, *14*, 4852.
61. Tan, X.; Li, Q.; Yang, J.; *Spectrochim. Acta, Part A* **2020**, *224*, 117356.
62. Gao, F.; Zheng, D.; Tanaka, H.; Zhan, F.; Yuan, X.; Gao, F.; Wang, Q.; *Mater. Sci. Eng., C* **2015**, *57*, 279.

Submitted: July 30, 2021
Published online: November 25, 2021